Experimental Definition of Nonaxisymmetric Exhaust Nozzle Plumes

Michael Compton* and Douglas Bowers†
Air Force Wright Aeronautical Laboratories, Wright-Patterson Air Force Base, Ohio

A detailed steady-state five-hole cone probe pressure survey of vectored and nonvectored exhaust plumes was conducted in the AFWAL Trisonic Gasdynamics Facility. Data were collected at a freestream Mach number of 0.5 for a convergent nozzle with an aspect ratio of 11 that was integrated into the wing trailing edge of a half-span wing/body configuration. Selected cross-sectional pressure and Mach number maps between 0 and 40 nozzle heights downstream are presented. Analysis indicates that the vectored nonaxisymmetric exhaust plume exhibits an accelerated rate of mixing and diffusion, primarily the result of a component of the jet in crossflow rather than the influence of the wing/body flowfield.

Nomenclature

$\mathcal{R}$ = aspect ratio
C_L = lift coefficient
D = average nozzle height, = 0.16 in.
M_L = local Mach number
NPR = nozzle pressure ratio
P_b = probe lower pressure, psfa
P_l = probe left‡ pressure, psfa
P_p = average of probe pressures, top, bottom, left, right
P_r = probe right‡ pressure, psfa
P_{s0} = tunnel static pressure, psfa
P_{s_p} = calibrated probe static pressure, psfa
P_t = probe top pressure, psfa
P_T = tunnel total pressure, psfa
P_{T0} = tunnel total pressure, psfa
P_{Tp} = probe total pressure, psfa
U = local velocity, ft/s
U_c = centerline velocity, ft/s
U_M = nozzle exit velocity, ft/s
x = coordinate axis parallel to tunnel centerline
Y = coordinate axis perpendicular to wing planform
Y' = $Y/(D/2) = 1$ at upper nozzle surface, -1 at lower nozzle surface
Z = coordinate axis perpendicular to the tunnel centerline and wing planform
α = angle of attack
β = yaw angle
Δ = difference

Introduction and Background

THE study of exhaust plumes began with the work of researchers in the mid-1950s focusing on cold jets exhausting into quiescent air.[1-3] Areas investigated included jet noise, jet boundary, and applications of the method of characteristics. The late 1950s through the mid-1960s saw studies of hot plume gases, rocket plumes, simple wing bodies with exhaust plumes at supersonic speeds, and initial studies of VTOL nozzles (e.g., Refs. 4 and 5). This period also introduced the first study of rectangular nozzles, primarily for VTOL. Since then a number of researchers have measured or calculated the characteristics of three-dimensional exhaust jets[6-10,16] with the primary emphasis on aircraft noise and mixing and, more recently, the plume structure for determining plume infrared emissions.

Recognizing the increasing importance of this technology to tactical aircraft propulsion integration, it was determined that a need existed for an investigation of nonaxisymmetric exhaust plumes issuing from a generic advanced-aircraft configuration. The Air Force Wright Aeronautical Laboratories initiated this integrated exhaust nozzle plume investigation with the objective to 1) establish an empirical data base applicable to the nonaxisymmetric plume technology, 2) provide experimental results for comparison with and subsequent improvements to existing analytical techniques, and 3) generally enhance the in-house level of knowledge and understanding of nonaxisymmetric vectored vs nonvectored plume characteristics.

This paper describes the approach taken and the apparatus utilized in the study and discusses the various observations made during the analysis of the data. Selected data for two plumes, both issuing into Mach 0.5 freestream at a nozzle pressure ratio (NPR) of 3.0 are presented and discussed. A technical report containing the complete data base of over 11,000 test points investigating boundary definition, plume spreading, flow angularity, velocity, Mach number, and pressure distributions can be obtained by submitting a request to the Aeromechanics Division, Flight Dynamics Laboratory.

Facility/Model/Test Description

The Trisonic Gasdynamics Facility at Wright-Patterson Air Force Base is a closed-circuit, variable density, continuous flow wind tunnel with an operating Mach number range of 0.23-3.0. For subsonic tests, a 2×2 ft solid wall test section is installed. The half-span model, shown in Fig. 1, is a wing/body configuration with interchangeable exhaust nozzles integrated into the wing trailing edge near the root. The wing has a leading-edge sweep of 40 deg and a trailing-edge sweep of 12.6 deg, with a NACA 63A206 section at the root and a NACA 65A204 section at the wing tip. This model provided a quick and simple means of investigating the developmental characteristics of a jet exhaust plume issuing from a generic airframe propulsion system integration into a nonquiescent freestream.

Presented as Paper 83-1290 at the AIAA/SAE/ASME 19th Joint Propulsion Conference, Seattle, Wash., June 27-29, 1983; received July 5, 1983; revision received Dec. 3, 1984.

*Aerospace Engineer, Airframe-Propulsion Integ. Group; Lieutenant, U.S. Air Force.

†Aerospace Engineer, Airframe-Propulsion Integ. Group.

‡Right and left sides of probe when viewed from an upstream location.

The schematics of both the vectored and nonvectored nozzle hardware used in this investigation are shown in Fig. 2. An aspect ratio of 11 was determined for both nozzles from the ratio of nozzle width to average nozzle height at the exit plane. Both nozzles were similar with the exception of the last 5% of the vectored nozzle chord in which the nozzle surfaces were turned through 15 deg to provide a vectored exhaust stream. For optimum wing and trailing-edge integration, the nozzle exit geometry was trapezoidal in shape. The nozzle exit height at the outboard station was 46% of the station furthest inboard. In addition, three flow-turning vanes were located inside of the nozzle hardware between the model plenum chamber and the nozzle exit (Fig. 3). These vanes were necessary because they provided structural integrity to the nozzle hardware and flow turning of the jet exhaust. As discussed below, these vanes, which are similar to modern nozzle flow control concepts, significantly distorted the nozzle internal flow. Freestream flow conditions were held constant at Mach = 0.5, with a nominal cold jet NPR of 3.0 and an operating Reynolds number of 2.0×10^6/ft. For the nozzle pressure ratio investigated, the convergent nozzle was moderately underexpanded with a small region of supersonic flow near the nozzle exit.

The instrumentation consisted of a five-port conical pressure probe and a five-component strain gage balance that measured the forces on the entire model. Extensive propulsion/aerodynamic parametric tests with this model are reported in Refs. 10, 11, and 15.

Survey Probe Description and Calibration

The plume survey was accomplished using a miniature five-port conical miniprobe developed by the Chrysler Michoud Defense Space Division. The small probe created minimal interference, while providing discrete flow measurements of pressure and flow angularity. Turbulence, velocity, and temperature measurements, useful for computational verification, were not obtained in this test entry. These measurements are to be obtained in subsequent test entries using hot-wire anemometry, laser Doppler velocimetry (LDV), and thermocouples.

Although velocity and static pressures were not directly measured, approximations can be derived from the probe calibrations and isentropic flow relations. With local Mach numbers expected to range from low subsonic to Mach 1.5, several pre- and post-test calibrations were conducted in order to obtain 1) the effect of Mach number on average "static" to pitot pressure ratios at $\alpha = 0$ and 2) the effect of pitch and yaw variations at various Mach numbers on the ratio of the "static" pressure difference to the pitot pressure. Independent calibrations of α and β were conducted to angles as large as 40 deg over a Mach range of 0.3-1.5. Limitations in the movement capabilities of the tunnel sting support mechanism prevented acquisition of combined α and β flow inclination data. Without these data, cross-coupling-induced errors as large as 10% could be present.[14,15] However, first approximations of local Mach number and flow angularity can be determined and the local static pressure is derived via the following process: given the four conical surface pressures as well as the pitot pressure at a given data point, the ratio of the average cone surface pressure to the pitot pressure is determined. From the calibration data determine the first approximation ($\alpha = 0$) of the local Mach number. Then, using the pitch and yaw plane pressure difference, determine the pitch and yaw components of the flow, using the angularity results interpolated between the closest descrete Mach numbers for which the angularity calibration data were obtained. The Mach number and flow angularity measurements are accurate only for low turbulence and small gradients of pressure and velocity. Therefore, the confidence levels of the Mach number and flow angularity results are lowest near the nozzle exit plane where large velocity and pressure gradients exist and near the plume boundary where large velocity and pressure gradients exist in combination with the high turbulence levels normally associated with the mixing layers. In these regions, illustrated in Fig. 4, Mach number and angularity results were excluded from the numerical analysis. However, in some cases, the local Mach number was determined if the pressure ports used in the averaging process were within the same pressure field as the total pressure orifice.

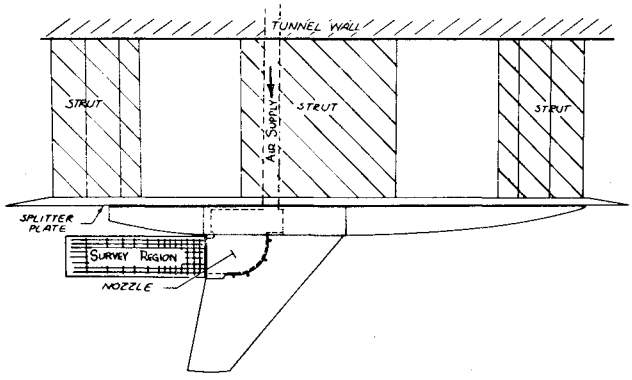

Fig. 1 Schematic of half-span model and test setup.

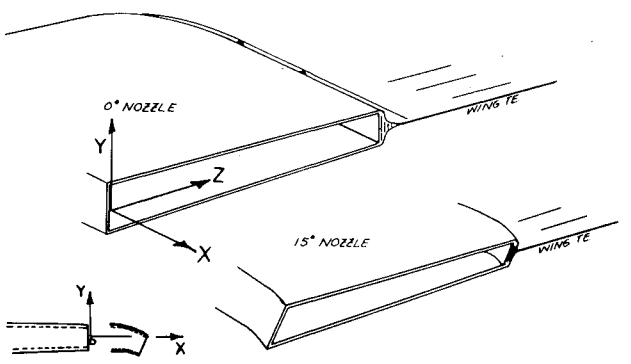

Fig. 2 Sketch of nonvectored and vectored integrated nozzles.

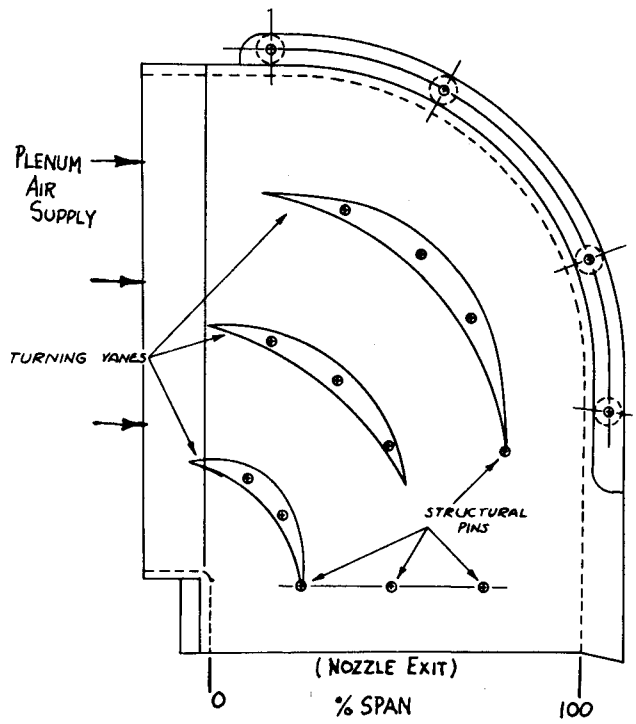

Fig. 3 Planform view of the internal nozzle structure.

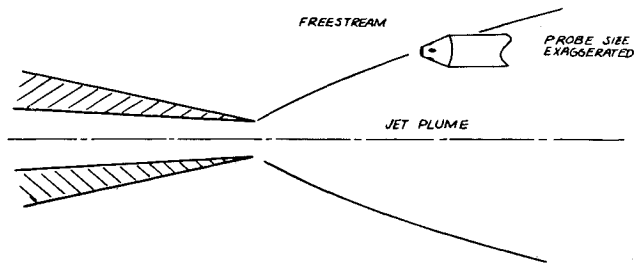

Fig. 4 Probe "straddling" the plume boundary.

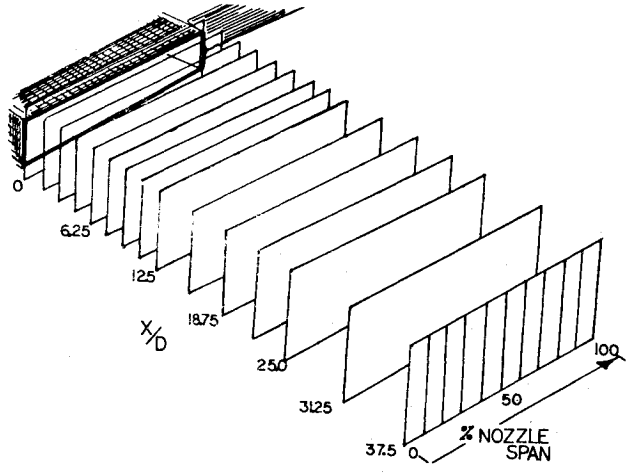

Fig. 5 Survey planes relative to the nozzle exit.

Plume Survey Details

As illustrated in Fig. 5, each plume was divided into 15 cross sections in the downstream direction. The cross sections were taken in 0.25 in. increments near the nozzle, 0.5 in. increments midway, and 1.0 in. increments farthest from the nozzle. At each cross section, the cone total and conical surface pressures were gathered at 11 spanwise stations from the inboard edge of the nozzle to a station slightly outboard of the nozzle opening. The test point density was 40-100 points/in., depending on the location of the probe in the plume. The computer moved the probe to a scheduled X-Y-Z location, monitored the change in the probe total pressure, recorded the data, and moved the probe to the next location. Data were recorded automatically once the rate and magnitude of pressure changes fell below prescribed values.

The intent of the survey was to concentrate measurements within the plume. Thus, a flow parameter that would accurately indicate the plume boundary was necessary. The flow parameter chosen was the ratio of probe total pressure to freestream total pressure. Other boundary parameters ($\frac{1}{2}U_c$, etc.) are dependent on variables that were not directly measured and the use of calculated quantities could introduce unacceptably large errors. A total pressure ratio of 1.0 indicated the immediate presence of either the transition between plume and the wing wake or between the wing wake and the freestream. These two flowfields were easily discernable near the nozzle exit and became less discernable as the mixing layer developed.

Discussion of Results

The remainder of this paper is devoted to a discussion of various observations made during the analysis of both the nonvectored and vectored plumes. For this paper, the discussion is limited to a comparison of the vectored to nonvectored selected pressure and Mach number results at $X/D=0$ and 25 only. The complete data set includes 14 other cross-sectional planes.

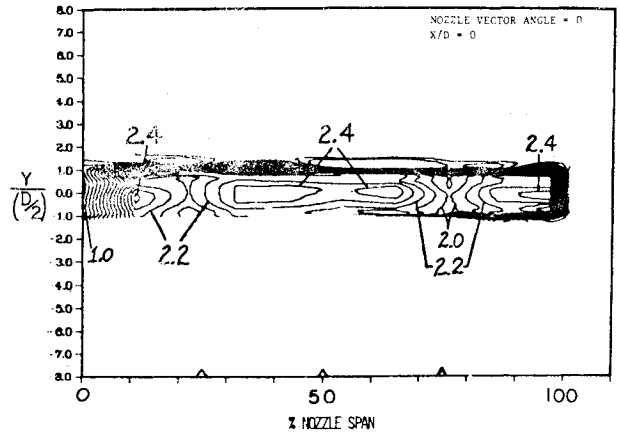

Fig. 6 Y-Z total pressure distribution at $X/D=0$, nonvectored.

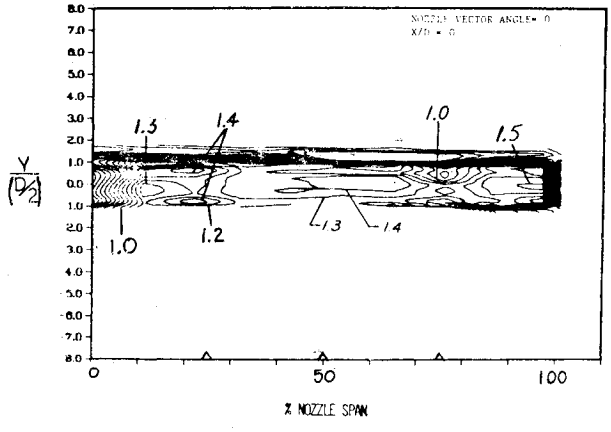

Fig. 7 Y-Z Mach number distribution at $X/D=0$, nonvectored.

In each plot presented, the downstream distances shown are nondimensionalized by the mean nozzle height D. All dimensions in the Y direction are nondimensionalized by $D/2$ so that the ordinate values of 1 and -1 correspond to the upper and lower nozzle exit surfaces, respectively. Spanwise directions are nondimensionalized by the length of the nozzle span to show the percent nozzle span. All vectored and nonvectored survey planes were vertical relative to the tunnel centerline and, although these planes were nearly perpendicular to the nonvectored total pressure centerline, they were inclined to the vectored plume centerline by as much as 15 deg in the proximity of the nozzle exit.

Nonvectored Plume

Figures 6 and 7 show the nonvectored plume total pressure and Mach number contours in the Y-Z plane at the nozzle exit. The total pressure contours (Fig. 6) indicate that there are four small high-pressure regions. The location of these high-pressure cores correspond to the location of the spaces between the internal nozzle turning vanes shown earlier in Fig. 3. (The triangular marks on the abscissa show the relative spanwise locations of the turning vanes.) These vanes appear to have a similar influence on the Mach number distribution (Fig. 7). It should be noted that plume total pressures appear to be generally more uniform and show a more even spatial distribution than observed in the Mach number. This can also be seen in the X-Y cross-sectional views of total pressure and Mach number (Figs. 8 and 9). This suggests that the static pressure distribution is dissimilar to that shown in total

pressure, particularly between the 0 and 8 nozzle heights downstream. The dissimilarity seems to diminish considerably just downstream of the supersonic cells. A sonic region at approximately 2.5 nozzle heights downstream separates the two supersonic cells. This is most likely the first shock intersection point separating the supersonic cells typically found in underexpanded jets of sufficiently large NPR.

A cross section through the pressure and Mach number contours at 25 nozzle heights downstream (shown by the dashed lines in Figs. 8 and 9) results in the *Y-Z* sectional views shown in Figs. 10 and 11. Note that in Fig. 10, which shows the total pressure distribution, a pressure deficit is visible at the 75% nozzle span that is probably the result of the wake from the outboard vane. This figure also shows an inboard and slightly upward displacement of the plume contours. The latter effect is probably the result of the exhaust flow "following" the contours of the model aft end. Figure 11 shows the Mach number distribution at the same cross section. The absence of an outboard Mach core similar to the core observed in total pressure plot suggests that, at this downstream station, the local static pressure distribution is dissimilar in character to the total pressure distribution.

Figure 12 shows the centerline velocity ratio vs downstream *X/D* at the midspan location plotted on a semilogarithmic scale. From Krothapolli,[8] a slope of approximately zero is identified as the potential core region in which the axial component of velocity is nearly invariant. A second region with a slope of -0.5 is defined as the region in which the velocity decays at a rate nearly the same as that of a planar flow or a two-dimensional region. A third region with a slope of -1 was defined as the axisymmetric region in which the velocity decays at a rate nearly that of an axisymmetric jet. The current data show a nearly invariant velocity ratio between the nozzle exit and approximately 6.5 heights downstream suggesting that this is the potential core region. This is consistent with earlier observation that the flow is supersonic to an *X/D* of approximately 7 when the transition to fully viscous flow occurs. Between *X/D* of approximately 6.5 and 17, a slope of approximately -0.45 was measured, closely approximating the decay rate of two-dimensional jets. Beyond and *X/D* of 17, however, the present experimental results yield nearly invariant velocity ratios up to the limits of the investigation.

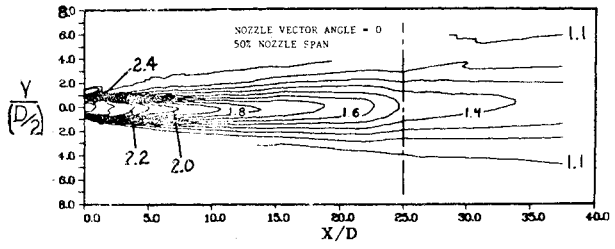

Fig. 8 *X-Y* total pressure distribution at the midnozzle span, nonvectored.

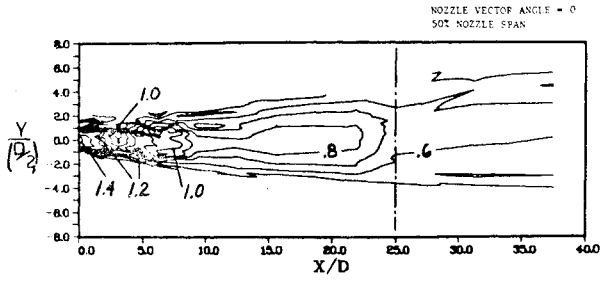

Fig. 9 *X-Y* Mach number distribution at the midnozzle span, nonvectored.

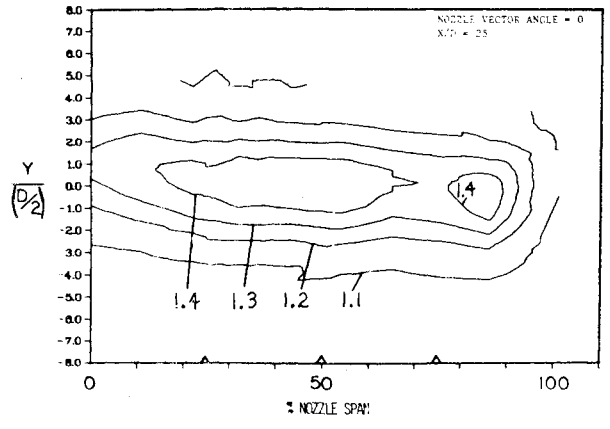

Fig. 10 *Y-Z* total pressure distribution at *X/D* = 25, nonvectored.

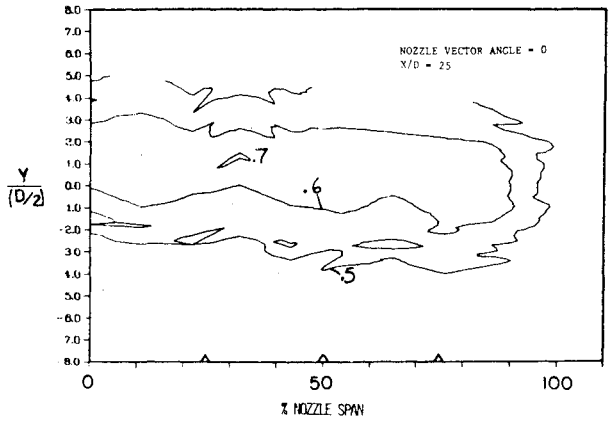

Fig. 11 *Y-Z* Mach number distribution at *X/D* = 25, nonvectored.

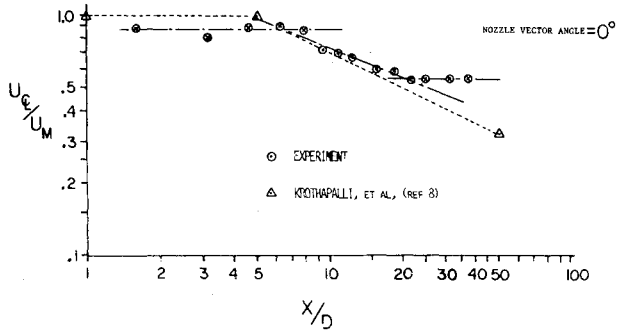

Fig. 12 Logarithmic plot of centerline velocity ratios, nonvectored.

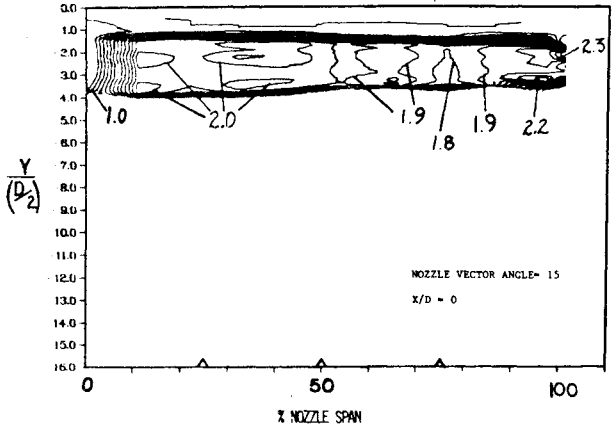

Fig. 13 *Y-Z* total pressure distribution at *X/D* = 0, vectored.

This is completely unexpected and implies that plume growth and momentum transfer to the surrounding fluid is nonexistent. Certainly, this is not the case. Assuming the equations and data are correct, there must be some outside influence on the section of plume from which these measurements were taken. A possible explanation was found in a sample of Marsters' work.[16] Marster's study focused on the determination of the plume from an array of very closely spaced two-dimensional nozzles. The velocity ratios vs normalized downstream distances presented are quite similar to those determined in the present investigation. The similarities not only include the slopes, magnitudes, and trends of data in the potential cores and planar flow regions, but also the downstream stations at which Marster's data depart from isolated single-nozzle data. This suggests that the flow issuing from the nozzles in the present experiment is more like flow issuing from several closely spaced nozzles rather than a single high $\mathcal{R}$ nozzle. It seems likely that such a condition existed at the nozzle exit. The resultant flow would then take on the exit plane pressure profiles observed and discussed earlier, as well as yield centerline velocity ratios similar to those obtained from an array of closely spaced nozzles.

Vectored Plume

Figures 13 and 14 show total pressure and Mach number contours for the *Y-Z* survey plane closest to the nozzle. Analysis of these and similar plots for other downstream locations indicate that, once again, static pressure nonuniformities exist, but do not appear to be as strong as those in the nonvectored plume. There is also an indication that the turning vanes have again induced distortion in both the total pressure and Mach number, although not to the level observed in the nonvectored plume. Similarly, the most outboard turning vane seems to exhibit the largest influence on the jet, particularly in Mach number. Figure 14 shows the Mach numbers in the vicinity of each of the turning vanes, with the largest region existing near the outboard vane. Overall, a large area of transonic flow existed near the vectored exit nozzle plane. This region of transonic flow can be observed in Fig. 15, which shows the Mach number distribution in a vertical plane at the midnozzle span. Both upper and lower regions of supersonic flow extend to an *X/D* of approximately 2.5, compared to 7 in the nonvectored plume.

The total pressure distribution at the same station is shown in Fig. 16. A comparison of Figs. 15 and 16 indicates that there is little similarity between the Mach number and the total pressure contours. This dissimilarity over the entire downstream distance investigated suggests that there exists a much greater nonuniformity in static pressure than observed in the nonvectored plume.

A comparison of Figs. 16 and 8 indicates that, with the exception of the curvature of the total pressure centerline, the very uniform total pressure distribution is similar in shape to that observed in the nonvectored plume. However, the comparison yields two noticeable differences. The first is that at each downstream station the centerline total pressure value in the vectored plume is less than the total pressure value at the same *X/D* in the nonvectored plume. Figures 17 and 18 show in the *Y-Z* cross section (at 25 nozzle heights downstream) peak vectored Mach numbers and total pressures of approximately 0.8 and 1.3, respectively, while peak nonvectored Mach numbers and total pressure values of 0.7 and 1.4 are seen in Figs. 10 and 11. The lower peak total pressures and higher peak Mach numbers suggest that, relative to the nonvectored pressures, the vectored static pressures are lower and closer to freestream values. It is hypothesized that the differences in pressures and Mach numbers between the vectored and nonvectored plumes are primarily the combined results of the separated flow and induced turbulence over the flap-like portion of the vectored nozzle and the cross flow component of the freestream.

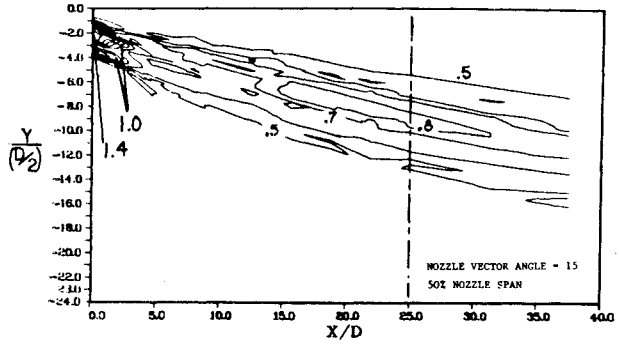

Fig. 15 *X-Y* **Mach number distribution at the midnozzle span vectored.**

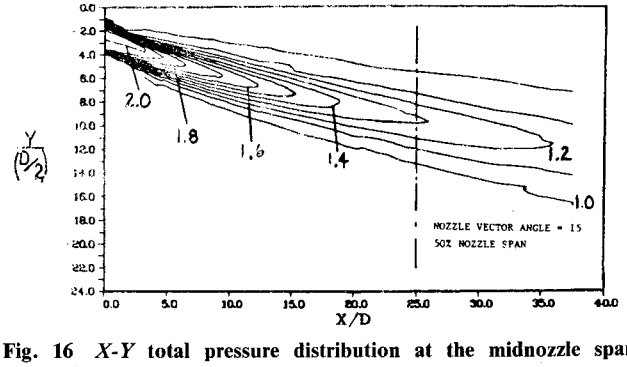

Fig. 16 *X-Y* **total pressure distribution at the midnozzle span vectored.**

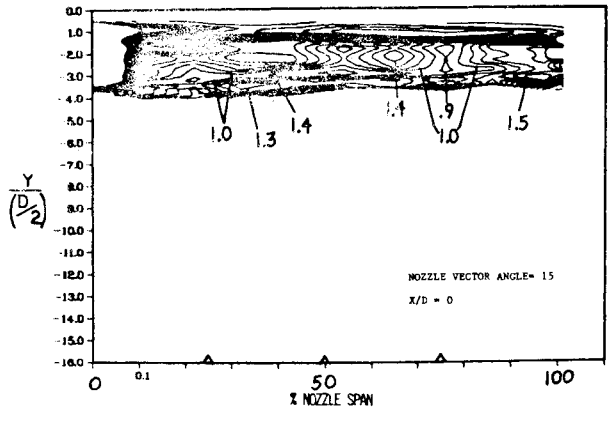

Fig. 14 *Y-Z* **total pressure distribution at** $X/D = 0$**, vectored.**

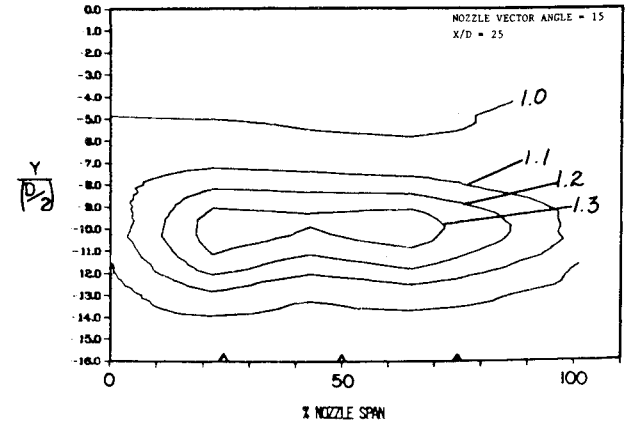

Fig. 17 *Y-Z* **total pressure distribution at** $X/D = 25$**, vectored.**

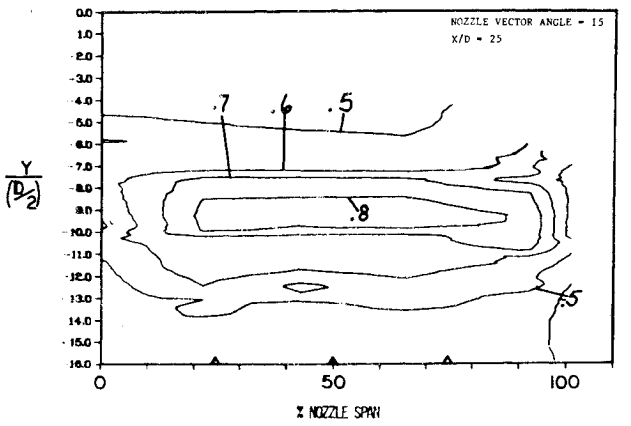

Fig. 18 *Y-Z* **Mach number distribution at** $X/D = 25$**, vectored.**

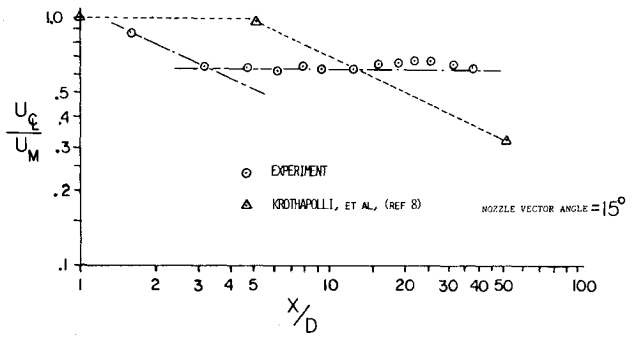

Fig. 19 Logarithmic plot of centerline velocity ratios, vectored.

Vectored plume centerline velocity data are shown on a semilogarithmic scale in Fig. 19. This data suggests that like the nonvectored plume, a region of two-dimensional flow (indicated by a slope of -0.5) exists at approximately 1-3 nozzle heights. Also, like the nonvectored plume, a region immediately downstream exists that indicates a near zero decay rate. Except for the explanation offered in the nonvectored case, the absence of a velocity decay rate is not understood. Again, like the nonvectored plume, there is no region containing flow described as axisymmetric in which the slope of the line approaches -1. Unlike the nonvectored data however, the potential core region is significantly smaller and closer to the nozzle exit, in agreement with an earlier observation regarding the reduced size of the supersonic region near the vectored nozzle exit. Finally, the extent of the region containing two-dimensional flow is significantly smaller than that observed in the nonvectored data. Again, both the flap-like flow separation and the associated increase in turbulence, as well as the cross flow influence, are thought to be responsible for the differences in the velocity centerline data.

A comparison of Figs. 17 and 10 illustrates the freestream flow influence on the peripheral regions of the plume. Unlike the generally symmetric distribution of total pressure above and below a horizontal plane of symmetry at $Y' = \frac{1}{2}$, the region of the vectored plume containing total pressure ratios between 1 and 1.1 in Fig. 17 appears to be asymetrically distributed. The asymmetry is most evident between nozzles spans of 0-10% and 80-100%. At the same station, Fig. 18 shows a similar asymmetry in the Mach number distribution of regions containing values less than 0.7. The resultant contours shown in Figs. 17 and 18 and visible in all the vectored pressure and Mach number maps are qualitatively similar to the jet in cross flow influence of the freestream on a noncircular plume shown in Ref. 19. Although the results shown in Ref. 19 apply to smaller $\mathcal{R}$ nozzle flows issuing at right angles to the freestream, the same shaping influence of the nonparallel freestream on the noncircular plume is present. However, one difference is that the influence does not appear to be symmetrical about the nozzle midspan. The contours at the outboard nozzle span are not surprising, as they generally reflect the shaping influence of the cross flow on the vectored exhaust stream. However, the inboard contours reflect an influence different from that observed at the outboard nozzle station. The asymmetry of the contours at the inboard and outboard nozzle stations was not expected and is not completely understood. Two possible explanations seem reasonable. The first is that the portion of the jet furthest inboard is issuing into a wing/body boundary layer. As a result, the inboard sections of the jet plume are not exposed to the same plume shaping influence as the outboard sections of the jet. Another explanation might be that the asymmetry is the result of the nonuniform mass flow, Mach number, and pressure distributions across the nozzle span. The higher-energy regions of the exhaust would be less influenced by the freestream crossflow component. It seems likely, however, that there are several contributing factors occuring simultaneously to provide the net effect of the cross sectional asymmetry.

Conclusions

An investigation of vectored nonaxisymmetric plumes exhausting from a highly integrated convergent nozzle into a Mach 0.5 freestream was conducted with the objective to 1) establish an empirical data base applicable to the nonaxisymmetric plume technology, 2) provide experimental results for comparison with and subsequent improvements to existing analytical techniques, and 3) generally enhance the in-house level of knowledge and understanding of nonaxisymmetric vectored vs nonvectored plume characteristics. Two plumes were studied, one issuing from a 0 deg vectored nozzle and the other from a 15 deg vectored nozzle. Just over 11,000 tests points were collected, 6000 for the nonvectored and 5000 for the vectored plumes. The characteristics of both plumes studied included boundary definition, plume spreading, flow angularity, velocity, Mach number, and pressure distributions, although only selected portions of the pressure and Mach number results are presented in this paper. The model tested was not intended to be representative of any particular tactical or strategic configuration. The generic half-span hardware was used because it was available hardware and because it provided the opportunity to gather the type of data necessary to meet the test objectives.

The following conclusion/observations can be drawn from the investigation:

1) Flow turning vanes inside both nozzles produced distorted total pressure and Mach number maps. The distortion is most obvious at downstream stations close to the nozzle exit plane. Four high-pressure cells are most visible at the exit plane. Calculated downstream velocity ratios suggest that the flow exiting this nozzle is similar to four closedly spaced, lower $\mathcal{R}$ nozzles.

2) The plume centerline velocity ratio plots also indicated that potential core and planar flow existed in both the nonvectored and vectored plumes with the transition from the former to the latter occurring slightly earlier in the vectored plume. However, velocity ratios indicative of axisymmetric flow were not found in the regions investigated. A similar observation was found in Marsters' studies.[16]

3) The short and deflected section of the vectored nozzle induced increased jet mixing, as illustrated by the differences between the flow conditions at both nozzle exit planes. Increased mixing throughout the rest of the vectored plume is believed to be primarily the result of a "jet in cross flow" component of the freestream flow perpendicular to the local vectored plume centerline.

References

[1]Love, E.S., Woodling, M.J., and Lee, L.P., "Boundaries of Supersonic Axisymmetric Free Jets," NACA RM L56G18, 1956.

[2]Rousso, M.D. and Baughman, L.E., "Spreading Characteristics of a Jet Expanding from Choked Nozzles at Mach 1.91," NACA TN 3836, Dec. 1956.

[3]Love, E.S. and Grigsby, C.E., "Some Studies of Axisymmetric Free Jets Exhausting from Sonic and Supersonic Nozzles into Still Air and into Supersonic Streams," NACA RM L54L31, 1954.

[4]Higgins, C.C. and Wainwright, T.W., "Dynamic Pressure and Thrust Characteristics of Cold Jets Discharging from Several Exhaust Nozzles Designed for VTOL Downwash Suppression," NASA TN D-2263, April 1964.

[5]Snedeker, R.S. and Donaldson, C.D., "Experience on Free and Impinging Underexpanded Jets from a Convergent Nozzle," Aeronautical Research Associates of Princeton, Inc., Advanced Research Projects Agency Rept. 63, Sept. 1964.

[6]Chu, C. W. and Der, J. "Modeling of 2D-Nozzle Plume for IR Signature Prediction Under Static Conditions," AIAA Paper 81-1108, June 1981.

[7]Chu, C.W., Der, J., and Wun, W., "A Simple 2D-Nozzle Plume for IR Analysis," AIAA Paper 80-1808, Aug. 1980.

[8]Krothapalli, A., Baganoff, D., Karamcheti, K., "On the Mixing of a Rectangular Jet," *Journal of Fluid Mechanics,* Vol. 107, July 1980, pp. 201-220.

[9]Sfeir, A., "Investigation of Three Dimensional Turbulent Rectangular Jets," AIAA Paper 78-1185, July 1978.

[10]Bowers, D.L. and Buchan, F., "An Investigation of the Induced Aerodynamics Effects of a Vectored Non-Axisymmetric Exhaust Nozzle," AIAA Paper 78-1082, July 1978.

[11]Bowers, D.L., "Propulsive Aerodynamics of an Advanced Nozzle/Forward Swept Wing Aircraft Configuration," AIAA Paper 80-1158, July 1980.

[12]Vahl, W. and Weirich, R., "Calibration of 30° Inserted-Angle Core for Determining Local Flow Conditions in Mach Number Range of 1.51 to 3.51," NASA TN D-4679, Aug. 1968.

[13]Collins F.G., "Probe Techniques," *UTSI Short Course Notes,* University of Tennessee, Knoxville, Feb.-March 1979.

[14]Marsters, G.F., "Measurements in the Flow Field of a Linear Array of Rectangular Nozzles," AIAA Paper 70-0350, Jan. 1979.

[15]Bowers, D.L., "Aerodynamic Effects Induced by a Vectored High Aspect Ratio Nonaxisymmetric Exhaust Nozzle," *Journal of Aircraft,* Vol. 16, Aug. 1979, p. 515.

[16]Kamotani, Y. and Greler, I., "Experiments on a Turbulent Jet in a Cross Flow," NASA CR-72893, FT AJ/TR-71-62, June 1971.

[17]Adler, D and Baron, A., "Prediction of a Three-Dimensional Circular Turbulent Jet in Crossflow," *AIAA Journal,* Vol 17, Feb. 1979, pp. 168-174.